British Journal of Haematology, 1999, **104**, 288–295

Kinetic analysis of ^{52}Fe-labelled iron(III) hydroxide–sucrose complex following bolus administration using positron emission tomography

Soheir Beshara,[1] Hans Lundqvist,[2] Johanna Sundin,[2,3] Mark Lubberink,[2] Vladimir Tolmachev,[2] Sven Valind,[3,4] Gunnar Antoni,[3] Bengt Långström[3] and Bo G. Danielson[1] [1]*Department of Medical Sciences, Renal Section,* [2]*Department of Biomedical Radiation Sciences,* [3]*PET Centre, and* [4]*Department of Clinical Physiology, University Hospital, Uppsala, Sweden*

Received 20 April 1998; accepted for publication 23 October 1998

Summary. Kinetic analysis of a single intravenous injection of 100 mg iron(III) hydroxide–sucrose complex (Venofer®) mixed with ^{52}Fe(III) hydroxide–sucrose as a tracer was followed for 3–6 h in four generally anaesthetized, artificially ventilated minipigs using positron emission tomography (PET). The amount of injected radioactivity ranged from 30 to 200 MBq.

Blood radioactivity, measured by PET in the left ventricle of the heart, displayed a fast clearance phase followed by a slow one. In the liver and bone marrow a fast radioactivity uptake occurred during the first 30 min, followed by a slower steady increase. In the liver a slight decrease in radioactivity uptake was noted by the end of the study. A kinetic analysis using a three-compartment (namely blood pool, reversible and irreversible tissue pools) model showed a fairly high distribution volume in the liver as compared with the bone marrow.

In conclusion, the pharmacokinetics of the injected complex was clearly visualized with the PET technique. The organs of particular interest, namely the heart (for blood kinetics), liver and bone marrow could all be viewed by a single setting of a PET tomograph with an axial field of view of 10 cm. The half-life ($T_{1/2}$) of ^{52}Fe (8·3 h) enables a detailed kinetic study up to 24 h. A novel method was introduced to verify the actual ^{52}Fe contribution to the PET images by removing the interfering radioactive daughter ^{52m}Mn positron emissions. The kinetic data fitted the three-compartment model, from which rate constants could be obtained for iron transfer from the blood to a pool of iron in bone marrow or liver to which it was bound during the study period. In addition, there was a reversible tissue pool of iron, which in the liver slowly equilibrated with the blood, to give a net efflux from the liver some hours after i.v. administration. The liver uptake showed a relatively long distribution phase, whereas the injected iron was immediately incorporated into the bone marrow. Various transport mechanisms seem to be involved in the handling of the injected iron complex.

Keywords: positron emission tomography, ^{52}Fe, pharmacokinetics, liver uptake, bone marrow uptake.

The internal exchange of iron is largely concerned with three tissues: the erythron involved in the synthesis and maintenance of haemoglobin, the reticuloendothelial system which catabolizes and stores red cell iron, and the liver parenchyma which acts as an additional storage area for iron (Finch *et al*, 1970). Radiopharmaceuticals labelled with ^{52}Fe, ^{55}Fe or ^{59}Fe have been used in studies of iron metabolism (Robertson *et al*, 1983) and pharmaceutical iron preparations have been administered parenterally for therapy. However, the different parenteral iron preparations differ essentially in their complex stability, molecular mass, pharmacokinetics and toxicity (Geisser *et al*, 1992). The understanding of the *in vivo* behaviour of the iron(III)–hydroxide sucrose complex, which is increasingly used for the management of iron deficiency in the different clinical settings (Höchli *et al*, 1993; Mercuriali *et al*, 1993; Martini *et al*, 1994; Zimmermann *et al*, 1995, al-Momen *et al*, 1996; Silverberg *et al*, 1996), is required. Whether this complex is taken up by particular tissues and how readily available it is to the normal pathways of iron metabolism once it has entered tissues are questions of particular importance.

Correspondence: Dr Soheir Beshara, Department of Medical Sciences, University Hospital, S-751 85 Uppsala, Sweden.

Positron emission tomography (PET) is a general tracer technique based on the use of positron-emitting nuclides for labelling of a wide range of tracer molecules, e.g. metabolic substrates, receptor ligands or other compounds with physiological and biochemical qualities relevant to the study in question. With the aid of the PET technique, the dynamics of biological processes can be investigated *in vivo*. ^{52}Fe is a partial positron emitter with a half-life of 8·3 h. The distribution and kinetics of the labelled molecules in the different organs can easily be followed over time with PET equipment. PET tomographs therefore enable a quantitative evaluation of the tissue iron uptake, and by comparing this with blood iron kinetics the blood–tissue transport can be assessed.

^{52}Fe decays to ^{52m}Mn, which is also a positron emitter with a half-life of 21 min (Browne & Firestone, 1986). Thus the PET measurement represents a sum of the radioactivity from these two nuclides. For ^{52}Fe uptake measurements using PET, the values need to be corrected for the manganese radioactivity.

The aim of the study was to assess the pharmacokinetics of iron(III) hydroxide–sucrose complex by labelling the complex with ^{52}Fe and evaluating its clearance, uptake and distribution characteristics with the use of the PET technique.

METHODS

Laboratory animals. The experiments were performed on four female SPF Göttingen minipigs (Ellegårds Forsøgsgrise, DK-4261 Dalmose, Denmark) fasted overnight. They had a mean body weight ±SD of 21 ± 2·8 kg. After induction of anaesthesia by intramuscular injection of azaperone (2·2 mg/kg), zoleteil (6 mg/kg) and atropine sulphate (0·04 mg/kg), the animals were placed in the supine position and intubated for ventilation via an endotracheal tube. Oxygen and nitrous oxide, 35%/65%, were used for controlled ventilation and maintenance of arterial blood gases within the physiological range. Morphine (1 mg/kg) was administered intravenously prior to the surgical procedures, i.e. insertion of catheters into the internal jugular vein and carotid artery for tracer administration and blood sampling, respectively. A stable level of anaesthesia was maintained by continuous i.v. infusion of pentobarbital (8 mg/kg/h) and pancuronium bromide (0·25 mg/kg/h) in 1000 ml Rehydrex® (with a content of 25 g glucose, 2·6 g sodium chloride and 3·4 g sodium acetate). Arterial blood pressure, ECG, blood gases and serum levels of glucose and lactate were monitored every hour throughout the experiment. After the final measurement, the pigs were killed. The study was approved by the Ethics Committee for animal experiments of Uppsala University (Dnr C304/92, C63/96).

Radiopharmaceutical method. The cyclotron at the The Svedberg Laboratory, Uppsala, Sweden, was used to produce ^{52}Fe. Nickel powder of natural isotopic composition was pressed to a target pellet typically at 4 tons/cm^2. The target diameter was 14 mm and the thickness 0·7 g/cm^2. During proton irradiation, with 73–68 MeV protons and 7–10 μA, the targets were water cooled. The integrated beam currents during irradiation were 50–70 μAH.

The irradiated targets were dissolved in 10 ml of boiling concentrated hydrochloric acid, evaporated to dryness and redissolved in 10 ml of 8 M HCl under slight heating. Chlorine gas was passed through the solution for 3 min in order to transfer iron into the oxidation state 3$^+$. After oxidation, iron was twice extracted with di-isopropyl ether pre-equilibrated with 8 M HCl. The extract was washed at least twice with 10 ml of 8 M HCl. The final product was checked by gamma spectrometry to ensure that no traces of nickel or cobalt isotopes were present. ^{52}Fe(III) was then re-extracted in 3 × 5 ml of distilled water. The aqueous solution was evaporated to dryness and the iron was redissolved in 1 ml of 0·1 M HCl.

A complex of [^{52}Fe]Fe(OH)$_3$–sucrose was prepared according to the method developed by VIFOR International AG, Switzerland. 100 mg of sucrose was dissolved in the [^{52}Fe]FeCl$_3$ solution. The solution was sterile-filtered and NaOH (10 N) was added to adjust the pH to 11·8. Finally, 5 ml of iron(III) hydroxide–sucrose complex (Venofer®, 20 mg Fe/ml), containing 100 mg iron, was added to obtain the injection bolus, according to the description supplied by VIFOR Int., Switzerland.

The total amount of radioactivity given to the individual animal ranged from 30 to 200 MBq. The labelled complex was injected as a single intravenous bolus.

PET imaging. PET measurements were performed with a General Electric Medical System (GEMS) PC 2048-15 B or PC 4096-15 WB scanner. Both scanners produce 15 tomographic sections covering 10 cm in the axial direction, with a spatial resolution of approximately 6 mm within sections and a spacing of 6·5 mm between sections, measured as full width at half maximum. Images were reconstructed with the filtered back projection algorithm to a 128 × 128 matrix with a pixel size of 4 × 4 mm^2, using a 6 mm Hanning filter and corrected for physical decay of ^{52}Fe. Attenuation correction was based on transmission scans with a ^{68}Ga/^{68}Ge rotating pin radiation source. Transmission scans were performed before collection of emission data to verify proper positioning of the animal. In one of the animals, scans were obtained at three different positions, for visualizing the brain, the heart and the kidneys, whereas in the other pigs a standardized supine position was selected so that the heart, liver and thoracic vertebrae were situated in the field of view. The measurement times were 1 min for the first 15 frames and 15 min for the following frames. The tomograph was regularly calibrated against the ionization chamber and well counters.

Sampling. 16 blood samples of 2 ml each were drawn during the whole scanning procedure. Each sample was then immediately divided into two portions, 1 ml for use as whole blood and 1 ml for separation of plasma. The radioactivity in both the whole blood and plasma was then measured in a well counter that was cross-calibrated with the scanners. Samples of 2 ml each were drawn every hour for 4 h to correct for the influence of variation of the ^{52m}Mn concentration in the blood. The samples were left to stand for at least 1·5 h to allow a physical equilibrium between ^{52}Fe and ^{52m}Mn.

Correction of ^{52m}Mn in the blood. A complication when using ^{52}Fe in physiological studies is the radioactive

daughter ^{52m}Mn, which also emits positrons. The value obtained on PET measurement will thus constitute a sum of the radioactivity from these two nuclides. On administration of the complex, ^{52}Fe and ^{52m}Mn will be in physical equilibrium. They are extracted from the blood at different rates and a new equilibrium will be formed in blood *in vivo*. When a blood sample is taken for well counter measurement, this physiological equilibrium will be changed into a physical equilibrium with time. The time course of this change can be used to calculate the relative amount of ^{52m}Mn at physiological equilibrium.

After sampling, the radioactivity of ^{52}Fe in the blood sample is given by:

$$A_{Fe} = A^0_{Fe} \exp(-\lambda_{Fe} t) \quad (1)$$

where A^0_{Fe} is the iron activity at the time of sampling, λ_{Fe} is the decay constant of ^{52}Fe, and t is the time that has elapsed since sampling. The radioactivity of ^{52m}Mn in the blood sample can be written as:

$$A_{Mn} = A^0_{Mn} \exp(-\lambda_{Mn} t) + \frac{\lambda_{Mn}}{\lambda_{Mn} - \lambda_{Fe}} A^0_{Fe} \times [\exp(-\lambda_{Fe} t) - \exp(-\lambda_{Mn} t)] \quad (2)$$

where A^0_{Mn}; is the manganese radioactivity at sampling time and λ_{Mn} is the decay constant of ^{52m}Mn. The decay times are known and the equilibration time and the relative abundance of ^{52}Fe and ^{52m}Mn at physical equilibrium can be calculated. After sampling, the blood sample is immediately placed in a NaI(T1) well counter. At higher energies, a measuring window which gives information only about the radioactivity from manganese can be set. By analysing the increase in manganese radioactivity with time (Fig 1) by a simple fitting to equation (2), values of A^0_{Fe} and A^0_{Mn} which will give the ratio between these two radionuclides at the time of blood sampling will be obtained.

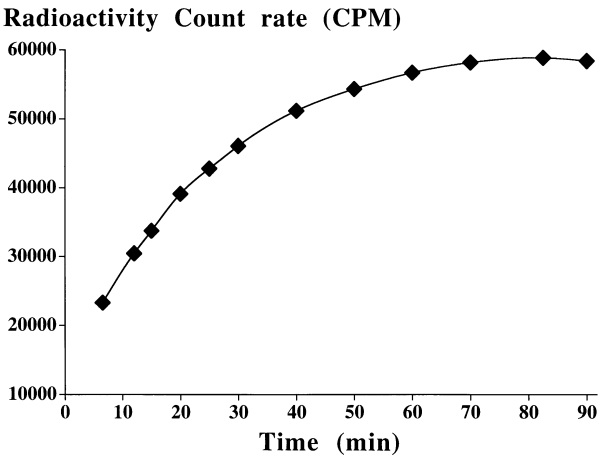

Fig 1. The count rate in the energy region above 1400 keV was measured in a NaI(T1) well-type detector, in a number of 1 min intervals during a 90 min period after collection of a blood sample. Count rates were plotted versus time after collection of the sample and the factor between ^{52m}Mn and ^{52}Fe radioactivity in the blood at the time of the sampling was calculated using a least squares fit of equation (2) to the data points.

Calibration procedure. A standard technique was applied for general calibration of the ionization chamber, tomograph and well counters. A known amount of ^{52}Fe (measured by a calibrated Ge detector) in physical equilibrium with ^{52m}Mn was measured by the ionization chamber. The radioactivity was evenly distributed in a cylindrical phantom (diameter 20 cm) with a known volume. Calibration factors were obtained by measuring the known radioactivity concentration by the tomograph. Samples with the known radioactivity concentration were then measured in the well counters in order to derive the proper calibration constants.

Data analysis: regions of interest (ROIs). After reconstruction, ROIs were selected and standardized as follows: ROIs in two or three slices of the liver were pooled to a volume of interest (VOI) of 6–8 cm^3. In the bone marrow a region with a total volume of about 4 cm^3, comprising 10 contiguous pixels of $4 \times 4 \times 6{\cdot}5$ mm^3/pixel, representing the highest radioactivity uptake in four different thoracic vertebrae, was chosen. A VOI measuring $1{\cdot}6$ cm^3 was selected in the centre of the left ventricle, where the measurement represented the blood radioactivity to assess the iron clearance, which could be compared later with data from the well counter measurement of the blood samples.

Analysis of time–activity and uptake data. Time–activity curves were obtained from the selected ROIs, taking into account the correction for decay and for ^{52}Fe/^{52m}Mn. Standardized uptake values (SUV) for the different organs were calculated as tissue radioactivity (MBq/cm^3) in relation to the injected activity per g body weight (MBq/g), assuming a tissue density of 1 (g/cm^3). Therefore the uptake reflected a dimensionless value which was comparable among the individual animals.

Graphical analysis. A general graphical method, used to analyse PET kinetic data, was then applied to determine the net influx from the blood to the tissues and also the sizes of the reversible pools (Rutland, 1979; Patlak *et al*, 1983; Patlak & Blasberg, 1985). With this method, functionally distinct compartments of tissue radioactivity are considered. The compartment may include multiple biochemical pools of iron. Functionally, they constitute a number of reversible compartments exchanging ^{52}Fe, and one irreversible trapping compartment where the tracer can enter but does not leave within the study period. The final slope does not resolve the various rate constants of which the steady state is composed. However, it is the useful constant since it represents the net clearance. After an initial distribution phase, during which the tracer is equilibrated between the blood and the reversible tissue compartments, the relationship between the tracer concentration in the blood and tissue may be described as:

$$C/C_b = V_d + K_t \int_0^t C_b(\tau) d\tau / C_b(t) \quad (3)$$

where the time courses of C (tissue concentration of the tracer) and C_b (blood concentration of the tracer) are measured from the tomographs and V_d is the fractional distribution volume of the reversible compartments, t is the real time in min after the administration of the tracer, K_t is the transfer rate constant into the irreversible compartment.

The integrated part of the equation constitutes a parameter of transformed time used to linearize the relationship between tissue and blood concentration. It has a dimension of time since it represents the time integration of blood curve divided by the blood curve itself. As C/C_b is a ratio between tissue and blood concentration of the tracer, it is therefore unitless, V_d is the fractional distribution volume, whereas K_t has units of a rate constant, min^{-1}. Equation 3 shows the resulting linear relationship between C/C_b and 'transformed time'. According to this model, the intercept of the linear part of the plot represents the distribution volume of the tracer in the reversible compartments of the tissue, and the slope represents the influx constant, i.e. a rate constant which describes the rate of transfer of iron from blood into the irreversible compartment. This transfer may also be seen as a clearance process, in which K_t represents volume of blood cleared/unit time/volume of tissue.

Statistical analysis. Data were analysed with the Excel SE + Graphics package (Microsoft Excel version 7.0, Microsoft Corporation, U.S.A.). The graphical method was applied to study the kinetics of ^{52}Fe in the liver and bone marrow. Since the equilibration time between the blood and the reversible compartments was unknown, the linear part of the plot was analysed by linear regression to obtain values of the slope and intercept. The linear regressions were calculated as a function of a number of data points starting from the last two data points and including more and more data points until stable values of slopes and intercepts were obtained.

RESULTS

Changes in the concentration of ^{52}Fe in the different tissues over time are shown in Fig 2.

Organ uptake

The time span in the kinetic studies varied in the animals from 3 to 6 h. In the first animal, which was studied while placed in different positions, large radioactive uptakes were observed in the liver and bone marrow. The brain scans showed no uptake, whereas the scans of the kidney showed a radioactivity concentration pattern which paralleled that of the blood, but the concentration was 30% higher than that in the blood. In the other animals, only one tomographic position was used to view the liver, thoracic vertebrae and heart.

Blood kinetics

Measurement of the radioactivity in the cardiac left ventricular blood pool in the tomographs gave a fair estimate of

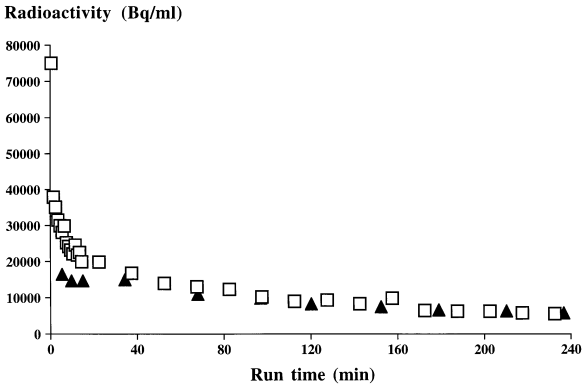

Fig 3. Comparison between the blood concentration of the radioactivity measured in the heart by the PET camera and the radioactivity measured in the blood samples: □, left ventricle activity, ▲, well counter activity.

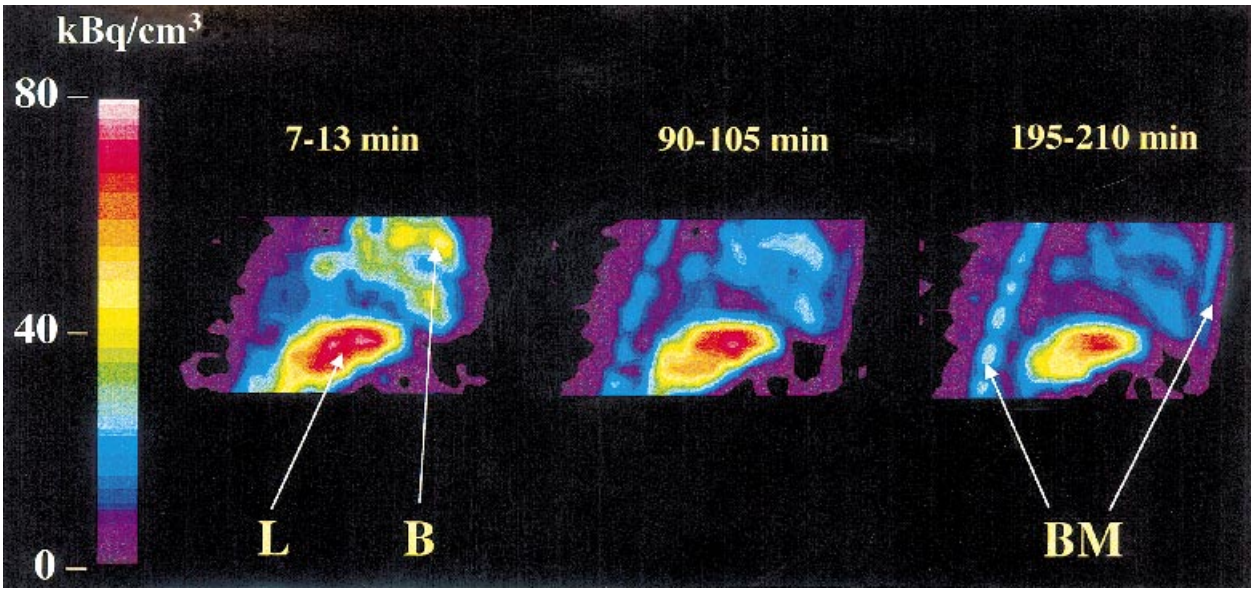

Fig 2. Changes in the concentration of ^{52}Fe in the tissues over time are shown in three PET tomographs in one of the pigs. L, liver; B, blood; BM, bone marrow.

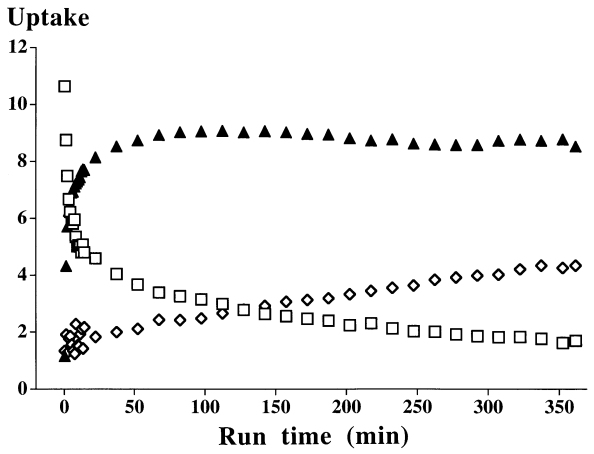

Fig 4. Representative uptake curves in the blood (□), liver (▲) and bone marrow (◇) in one of the pigs.

the blood radioactivity as shown by comparison with the blood samples (Fig 3). The radioactivity in the blood measured by PET in the left ventricle of the heart displayed a rapid clearance phase during the initial 10–20 min, followed by a slow clearance phase during the rest of the investigation period, reaching 20–25% of the peak activity by 4 h.

Liver kinetics

Fast radioactivity uptake was observed during the first 30 min, followed by a slow steady increase. A slight decrease in radioactivity was seen by the end of the study in some animals.

Bone marrow kinetics

In the bone marrow uptake curves, rapid radioactivity uptake was noted during the first 20 min, followed by a stable influx of the radioactivity into the bone marrow.

Representative uptake curves in the liver and bone marrow in one of the pigs are shown in Fig 4.

Correction for ^{52m}Mn activity in the blood

The activity ratio ^{52m}Mn/^{52}Fe in the blood was found to be in the range of 0·2–0·4. For further corrections, an average factor of 0·3 was used. Since the positron abundance for ^{52}Fe is 55·5% and for ^{52m}Mn 96·7%, the numbers of positrons emitted per ^{52}Fe decay at physical equilibrium should be 152·2%. In the blood the numbers of positrons per ^{52}Fe decay should then be $55{\cdot}5 + (0{\cdot}3 \times 96{\cdot}7) = 84{\cdot}5\%$. This is 0·56 times lower than during physical equilibrium. Therefore, when comparing tissue radioactivity concentrations, where ^{52m}Mn and ^{52}Fe can be assumed to be in physical equilibrium, with blood values obtained from the heart, these latter values should be divided by this factor.

Graphical analysis

In the curves where transformed time was used, a linear component was observed in the liver after 60 min. In the bone marrow, equilibration was very rapid and a straight line was found from the very beginning of the experiment. For the liver, data obtained at times >60 min were used in the linear regression, whereas for the bone marrow all data were used. The intercept of the linear part of the liver was fairly large, whereas that of the bone marrow very small. Results from the linear part of the linear regression are seen in Table I. Representative plots for the liver and bone marrow in one of the animals are shown in Fig 5.

DISCUSSION

The concept of internal iron exchange depends not only on a kinetic definition of exchange, but also on an anatomical localization and a functional explanation of this exchange (Cook *et al*, 1970). The PET technique has the advantages in allowing visualization of the distribution of the injected radioactive iron, and calculation of the rate of iron clearance.

The amount of radioactivity/body weight administered in this study is far in excess of the amounts that could be given

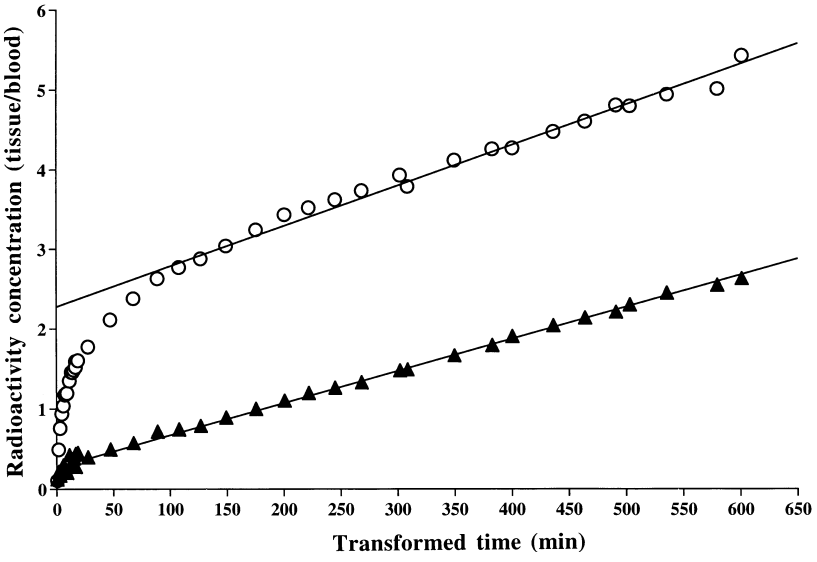

Fig 5. Representative plots of the graphical analysis in the liver (○) and bone marrow (▲) in one of the pigs. The radioactivity concentration on the *Y* axis is a ratio between tissue and blood, and therefore unitless, whereas the transformed time on the *X* axis represents the time integration of blood radioactivity curve divided by blood radioactivity itself, and therefore has the units of min. The intercept represents the factional distribution volume, and the slope represents the transfer rate constant from the blood to the trapping compartment.

Table I. Characteristics of the experimental set-up and results from the linear part of the graphical analysis.

Pig	Weight of pig (kg)	Injected activity (MBq)	Liver		Bone marrow	
			Distribution volume	Transport rate constant (min^{-1})	Distribution volume	Transport rate constant (min^{-1})
1	25	50	2·39	0·0150	0·77	0·0130
2	19	30	2·94	0·0110	0·30	0·0041
3	21	186	2·30	0·0051	0·27	0·0040
4	19	200	1·98	0·0042	0·23	0·0035

to man for such diagnostic purposes. This is because the animals were planned to be killed immediately after the experiments. Acceptable amounts for clinical investigations will give adequate information when applying the same technique.

The quantitative ability of the PET technique relies on proper calibration procedures. A particular problem in *in vivo* measurements of ^{52}Fe is the daughter ^{52m}Mn. The technique presented in this paper for measuring the relationship between ^{52m}Mn and ^{52}Fe in the blood is a useful way to compensate for this effect and allows quantitative kinetic information to be obtained. When iron is taken up by an organ, it will be mainly bound intracellularly. The ^{52m}Mn produced is then likely to be trapped at the site of its production and reflects the iron distribution. In tissues such as the bone marrow the intracellularly incorporated iron will, with time, produce ^{52m}Mn, which will also be expected to remain intracellularly. In tissues of this type a physical equilibrium between ^{52}Fe and ^{52m}Mn is likely to be established after some time. However, when iron decays in the blood the ^{52m}Mn produced will be freely distributable, following manganese kinetics. In PET measurements in the different tissues three sources contribute to the measured signal, namely ^{52}Fe, trapped ^{52m}Mn and freely distributable ^{52m}Mn. In our calculations we have disregarded the last factor and have assumed that the measured signal was provided by ^{52}Fe in physical equilibrium with ^{52m}Mn. This assumption is not applicable to measurements in the blood, where the removal of iron and manganese will be independent of each other and the equilibration will be dependent on the interaction between the decay and the tissue uptake. The distribution of freely distributable ^{52m}Mn was studied by Buck *et al* (1996), who reported rapid clearance from the blood, a finding consistent with our observation of a relatively low ^{52m}Mn content in the blood. The organs with the highest uptake were found by Buck *et al* (1996) to be the liver and the myocardium. In our study a relatively low myocardial uptake was noted after some hours, indicating that only a relatively small amount of the total ^{52m}Mn is free to be redistributed in the body. Therefore the liver is the organ that is expected to be most affected by the redistribution of ^{52m}Mn produced in the blood. The activity ratio, ^{52m}Mn/^{52}Fe, which at physical equilibrium should be close to 1, was found to be smaller and the numbers of positrons per ^{52}Fe decay were 0·56 times less than during physical equilibrium. The blood values obtained from PET measurements should therefore be divided by this factor. However, the radioactivity concentration in blood taken from the left ventricle was usually lower than the blood radioactivity measured in the well counter because of partial volume effects. Moreover, the correction factor might also be affected by the redistribution of ^{52m}Mn. An overall correction factor of 0·50 was therefore applied.

The left ventricular blood pool in the tomographs was chosen for measuring the blood radioactivity clearance. This gave a fair estimate, as shown by comparison with the blood samples. The advantages in choosing the left ventricle for this purpose were that the very early changes in blood kinetics could be visualized and frequent observations of ^{52}Fe in the blood could be made without withdrawing any blood from the subject. This is of special importance in anaemic patients. Moreover, the fact that measurements in the blood and tissues can be made in the same session simplifies the acquisition of data and the analysis, since most of the correction factors cancel out.

The uptake curves in the different organs, as assessed in the first pig in order to define the organs of interest, revealed an uptake of the radioactive iron by the liver and the bone marrow. This was in accordance with the major pathways of internal iron exchange as previously described (Finch *et al*, 1970). The parallelism between the uptake pattern in the renal tissue and the blood kinetics might mainly reflect uptake of ^{52m}Mn and to a much lesser extent uptake of ^{52}Fe. Less than 5% of the injected iron from the Fe(III) hydroxide–sucrose complex was found to be excreted in the urine (Danielson *et al*, 1996).

The graphical analysis provides two values: the distribution volume of ^{52}Fe equilibrating with ^{52}Fe in the blood, and the influx rate constant of ^{52}Fe to a compartment which binds ^{52}Fe irreversibly within the time frame of the study. However, PET measurements are affected by the redistribution of ^{52m}Mn in tissues both by an uptake of ^{52m}Mn from the blood and by decay of ^{52}Fe in tissues, as well as by calibration factors. Since free ^{52m}Mn will have kinetics close to that of the blood, in this analysis it will act as an extra high blood background. This will have its impact mainly on the intercept value, i.e. the distribution volume, and to a much lesser extent on the slope value. Dickinson *et al* (1996) found minimal uptake of ^{54}Mn by the bone marrow, which was in agreement with our findings of a very small intercept value

in the bone marrow. This, together with the low radioactivity uptake in the late measurements in the heart muscle, constitutes strong evidence that freely redistributing ^{52m}Mn disturbed the quantification to only a minor degree, especially at late times. A value of 3–4 at equilibrium was found for the radioactivity concentration ratio between the liver and blood of ^{52m}Mn as studied by Buck *et al* (1996). An estimate indicated that the liver uptake values might be overestimated by a maximum of 15–20% (Lubberink, personal communication). Nevertheless, the slope and intercept values were useful for inter-individual comparison.

An observation of interest in this study, which was performed *in vivo*, was that the blood to tissue (either liver or bone marrow) transfer rate constant was steady, irrespective of the large variation in the blood iron concentration over the range observed, i.e. a 4–5-fold variation from early to late points in time. This indicated that, despite the high doses of iron administered, saturation of the transport process was not reached. Various transport mechanisms of the injected iron complex are probably involved. These might include a rapid exchange with transferrin, with a subsequent increase in transferrin saturation and in the rate of its turnover. A rapid exchange of iron(III) hydroxide–sucrose complex to transferrin has been reported previously (Danielson *et al*, 1996). Near doubling of the iron turnover together with a higher erythroid marrow uptake has been reported to be obtained merely by increasing the plasma iron concentration, a finding attributed to a proportional increase in the amount of iron taken up by tissue transferrin receptor (Cazzola *et al*, 1985). This was in agreement with the results of our study, in which the absolute amount of iron transferred to the bone marrow was dependent on blood iron concentration, since the transfer rate constant of iron from the blood to the bone marrow was steady from the very beginning.

The blood radioactivity showed a rapid clearance phase followed by a slow one, probably indicating back transport of iron from the reversible compartment in the liver to the blood. A large reversible compartment was detected by the intercept value of the compartmental model in the liver, as compared to a fairly small one in the bone marrow. An earlier pharmacokinetic study of the complex showed an increase in serum ferritin levels within 8–10 h (Danielson *et al*, 1996). Direct endocytotic uptake of the iron(III) hydroxide–complex by the reticuloendothelial cells of the liver with subsequent synthesis of ferritin and its entry into the blood might contribute to the large reversible compartment in the liver. The reversible exchange of iron between the liver and the blood might explain the delayed steady state in the blood and liver kinetics as compared to the steadily increasing incorporation of iron into the bone marrow. On the other hand, the small intercept of the graphical analysis plot of the bone marrow indicates direct incorporation of the iron into the bone marrow with an almost negligible reversible pool. Direct endocytosis of the iron(III) hydroxide–sucrose complex by the marrow reticuloendothelial system may also be involved in marrow iron uptake.

Earlier ferrokinetic studies (Finch *et al*, 1970; Cook *et al*, 1970; Cazzola *et al*, 1985; Barosi *et al*, 1985) performed to study endogenous iron homeostasis were extremely helpful in the assessment of abnormalities in iron metabolism associated with various anaemic conditions. However, these models were hampered not only by being cumbersome and requiring repeated blood sampling, but also by the fact that they were based on assumptions which may not be all valid. In contrast, the PET measurements have the advantages of simultaneous quantification of blood and tissue uptake as well as the ability to derive transfer rate constants. The model used in the present study, even though aiming at analysing the pharmacokinetics of the iron(III) hydroxide–sucrose complex, can be applicable for tracer study as well and therefore may represent a valuable tool for the study of endogenous iron metabolism. Detailed information about the regional uptake of the injected complex was readily visualized using the PET technique. Therefore the model may also be useful in comparing the pharmacokinetics of different parenteral pharmaceutical iron preparations.

ACKNOWLEDGMENT

This work was supported by a Research Grant from Society for Renal Disease in the CUWX Counties.

REFERENCES

al-Momen, A.K., al-Meshari, A., al-Nuaim, L., Saddique, A., Abotalib, Z., Khashogji, T. & Abbas, M. (1996) Intravenous iron sucrose complex in the treatment of iron deficiency anemia during pregnancy. *European Journal of Obstetrics, Gynecology and Reproductive Biology*, **69**, 121–124.

Barosi, G., Cazzola, M., Berzuini, C., Quaglini, S. & Stefanelli, M. (1985) Classification of anaemia on the basis of ferrokinetic parameters. *British Journal of Haematology*, **61**, 357–370.

Browne, E. & Firestone, R.B. (1986) *Tables of Radioactive Isotopes*, p. 52. John Wiley & Sons, New York.

Buck, A., Nguyen, N., Burger, C., Ziegler, S., Frey, L., Weigand, G., Erhardt, W., Senekowitsch-Schmidtke, R., Pellikka, R., Bläuenstein, P., Locher, J.T. & Schwaiger, M. (1996) Quantitative evaluation of manganese-52m as a myocardial perfusion tracer in pigs using positron emission tomography. *European Journal of Nuclear Medicine*, **23**, 1619–1627.

Cazzola, M., Huebers, H.A., Sayers, M.H., MacPhail, A.P., Eng, M. & Finch, C.A. (1985) Transferrin saturation, plasma iron turnover and transferrin uptake in normal humans. *Blood*, **66**, 935–939.

Cook, J.D., Marsaglia, G., Eschbach, J.W., Funk, D.D. & Finch, C.A. (1970) Ferrokinetics: a biologic model for plasma iron exchange in man. *Journal of Clinical Investigation*, **49**, 197–205.

Danielson, B.G., Salmonson, T., Derendorf, H. & Geisser, P. (1996) Pharmacokinetics of iron(III)–hydroxide sucrose complex after single i.v. dose in healthy volunteers. *Drug Research*, **46**, 615–619.

Dickinson, T.K., Deveney, A.G. & Connor, J.R. (1996) Distribution of injected iron 59 and manganese 54 in hypotransferrinemic mice. *Journal of Laboratory and Clinical Medicine*, **128**, 270–278.

Finch, C.A., Deubelbeiss, K., Cook, J.D., Eschbach, J.W., Harker, L.A., Funk, D.D., Marsaglia, G., Hillman, R.S., Slichter, S., Adamson, J.W., Ganzoni, A. & Giblett, E.R. (1970) Ferrokinetics in man. *Medicine*, **49**, 17–53.

Geisser, P., Baer, M. & Schaub, E. (1992) Structure/histotoxicity relationship of parenteral iron preparations. *Drug Research*, **42**, 1439–1452.

Höchli, P., Wagenhauser, F.J. & Fehr, J. (1993) Repeated continuous administration of low doses of intravenous iron in anaemic patients with active rheumatoid arthritis. *European Journal of Haematology*, **51**, 54–55.

Martini, A., Ravelli, A., Di Fuccia, G., Rosti, V., Cazzola, M. & Barosi, G. (1994) Intravenous iron therapy for severe anaemia in systemic-onset juvenile chronic arthritis. *Lancet*, **344**, 1052–1054.

Mercuriali, F., Zanella, A., Barosi, G., Inghilleri, G., Biffi, E., Vinci, A. & Colotti, M.T. (1993) Use of erythropoietin to increase the volume of autologous blood donated by orthopedic patients. *Transfusion*, **33**, 55–60.

Patlak, C.S. & Blasberg, R.G. (1985) Graphical evaluation of blood-to-brain transfer constants from multiple-time uptake data: generalizations. *Journal of Cerebral Blood Flow and Metabolism*, **5**, 584–590.

Patlak, C.S., Blasberg, R.G. & Fenestermacher, J.D. (1983) Graphical evaluation of blood-to-brain transfer constants from multiple-time uptake data. *Journal of Cerebral Blood Flow and Metabolism*, **3**, 1–7.

Robertson, J.S., Price, R.R., Budinger, T.F., Fairbanks, V.F. & Pollycove, M. (1983) Radiation absorbed doses from iron-52, iron-55 and iron-59 used to study ferrokinetics. *Journal of Nuclear Medicine*, **24**, 339–348.

Rutland, M.D. (1979) A single injection technique for subtraction of blood background in ^{131}I-hippuran renograms. *British Journal of Radiology*, **52**, 134–137.

Silverberg, D.S., Blum, M., Peer, G., Kaplan, E. & Iaina, A. (1996) Intravenous ferric saccharate as an iron supplement in dialysis patients. *Nephron*, **72**, 413–417.

Zimmermann, R., Breymann, C., Richter, C., Huch, R. & Huch, A. (1995) rhEPO treatment of postpartum anemia. *Journal of Perinatal Medicine*, **23**, 111–117.